Optimized *in situ* crystal growth and disordered quasi-one-dimensional magnetism in Li$_2$Mn$_2$(MoO$_4$)$_3$

C. Franco,[1] A. Wustrow,[2] B. Xia,[1] A. M. Baccarella,[1] F. Burgos,[1] J. Nicasio,[1] E. Dooryhee,[3]
J. R. Neilson,[2] and J. W. Simonson[1,*]

[1]*Department of Physics, Farmingdale State College, Farmingdale, New York 11735, USA*
[2]*Department of Chemistry, Colorado State University, Fort Collins, Colorado 80523, USA*
[3]*National Synchrotron Light Source II, Brookhaven National Laboratory, Upton, New York 11973, USA*

The quasi-one-dimensional structure of Li$_2$Mn$_2$(MoO$_4$)$_3$ consists of three mutually distinct chains of Li$_{1-x}$Mn$_x$-centered polyhedra in which Mn ostensibly adopts a $J = 5/2$ Mn^{2+} configuration. *In situ* x-ray scattering experiments carried out as crystallites emerge from a molten oxide solution facilitate the synthesis of large single crystals. *Ex situ* x-ray diffraction finds no evidence of long-range Li/Mn occupancy ordering, suggesting that the structure is effectively composed of finite chains of Mn moments of statistically varying lengths. UV/visible diffuse reflectance spectroscopy measurements establish a wide 3.43(12)-eV direct charge gap consistent with the local polyhedral coordination of the nominally Mn^{2+} species. The temperature T dependence of the DC magnetic susceptibility χ reveals a fluctuating moment of only $2.74\mu_B \pm 0.01\mu_B$/Mn, dramatically reduced from the $5.9\mu_B$/Mn expected for Mn^{2+}. Meanwhile, the Weiss temperature $\Theta_W = -89 \pm 1$ K reveals antiferromagnetic fluctuations that are stymied from reaching an ordered state apparently by the chemical disorder intrinsic to the polyhedral chains. Measurements of magnetization vs field H at $T \leqslant 10$ K are far from saturation even at $H = 5$ T and are strongly non-Brillouin-like, instead scaling as $H/T^{0.24(3)}$ and suggesting the presence of quantum fluctuations associated with an eventual quasi-one-dimensional, disordered magnetic phase.

DOI: 10.1103/PhysRevMaterials.4.045404

I. INTRODUCTION

In low-dimensional or frustrated magnetic systems, quantum zero point fluctuations can be instrumental in determining the magnetic ground state [1]. In such materials, the combined effects of frustration and low dimensionality often reduce the energy scale of long-range magnetic order and give rise to novel or unconventional low-temperature magnetic states, including spin liquids, spin glasses, or quantum orbital spin chains [2].

Li$_{4-x}$M$_x$(MoO$_4$)$_3$-type compounds (M = Sc, V, Cr, Mn, Fe, Co, Ni, Cu, Zn, Al, or Ga) are examples of such compounds in which one-dimensional crystallographic motifs lead to high conductivities, fast ion transport channels, and, ultimately, potential technological applications [3–6]. These practically important properties stem in part from the low-dimensional, lyonsite-like structures often adopted by these phases and characterized by one-dimensional interstitial channels passing between vertex-sharing polyhedra and promoting the conduction of small cations like Li$^+$ and Na$^+$. In lyonsite-structured Li$_{4-x}$M$_x$(MoO$_4$)$_3$-type systems, these interstitial tunnels additionally serve to segregate infinite, parallel chains of Li/M face-sharing octahedra, Li/M edge-sharing octahedra, and Li/M edge-sharing trigonal prisms, providing three

distinct quasi-one-dimensional structural motifs, all arrayed along the same crystallographic direction [7].

Substitutional disorder between the Li and M sites is intrinsic across a wide swath of these systems and typically serves to stabilize the lyonsite structure while preserving electroneutrality [8]. Accordingly, when M is a valence-flexible $3d$ transition metal, its oxidation state and hence magnetic character can be controlled by the Li:M ratio. For instance, the temperature dependence of the magnetic susceptibility χ of Li$_3$Cr(MoO$_4$)$_3$ confirms the expected Cr^{3+} valence with an effective fluctuating moment of $3.91(1)\mu_B$/Cr and eventual weak ferromagnetism emerging below $T = 10$ K, perhaps due to short-range order [9]. Magnetic properties of the presumably mixed valent Li$_{1.8}$Cr$_{1.2}$(MoO$_4$)$_3$, however, have not been reported. Isostructural Li$_3$Fe(MoO$_4$)$_3$ reveals a similar Fe^{3+} oxidation state and corresponding weak ferromagnetism below $\sim$12 K [10,11]. On the other hand, the replacement of Li with a larger alkali metal like K or Rb obstructs the formation of mixed-occupancy sites, and their absence instead distorts the overall structure. Even so, exotic magnetic states can be achieved. In Rb$_2$Cu$_2$Mo$_3$O$_{12}$, for instance, the requirement for overall electroneutrality demands a $J = 1/2$ Cu^{2+} state, and two quantum critical regimes can be tuned with H at the upper- and lower-field boundaries of an ordered phase, with quasi-one-dimensional quantum fluctuations dominating above the high-H quantum critical point (QCP) [12]. Similarly, the $J = 1$ system Ni^{2+} ANi$_2$Mo$_3$O$_{12}$ (A = Rb or K) lacks substitutional disorder, is likewise distorted from the

---

*jack.simonson@farmingdale.edu

lyonsite structure, and engenders a correlated spin-1 tetramer ground state [13].

Naïvely, we could expect compositions with the largest moments and the greatest transition metal occupancies to yield the most robust magnetic states, as might be realized with $J = 5/2$ Mn^{2+}. Indeed, a detailed electron spin resonance (ESR) study on polycrystalline samples of $Li_2Mn_2(MoO_4)_3$ found the expected Mn^{2+} state along with the concomitant absence of any ESR signal corresponding to Mo ions, indicating the expected nonmagnetic Mo^{6+} configuration [14]. Most interestingly, χ measurements show a modest downturn below $T = 1.4$ K in this compound, which the study authors interpret as the onset of antiferromagnetism. It remains to be seen which of the three Li/Mn-centered polyhedral sites participate in this transition or whether the ordered state indeed corresponds to long-range antiferromagnetic order. Furthermore, it was very recently reported that $Na_2Mn_2(MoO_4)_3$ forms with a unique triclinic structure, and measurements of χ likewise suggest the onset of an antiferromagnetic ordered state at Néel temperature $T_N = 6.5(5)$ K [15].

We report here the results of *in situ* x-ray scattering experiments that have accelerated the synthesis of large, high-quality single crystals of $Li_2Mn_2(MoO_4)_3$ suitable for spectroscopic and magnetic measurements. Subsequent *ex situ* x-ray diffraction measurements confirm the expected composition $Li_{2.004(6)}Mn_{1.996(6)}(MoO_4)_3$ to high precision, indicating that integer stoichiometry is, indeed, favored by $3d^5$ Mn^{2+}, but bond valence sums uncover significant discrepancies from the ideal divalent state. UV/visible (Vis) spectroscopy reveals a wide gap consistent with the expected Mn atomic configuration, including multiplet features typically observed in octahedral MnO_6 systems. Finally, measurements of $\chi(T)$ divulge a paramagnetic fluctuating moment far smaller than the free-ion value, corroborating that a full picture of the Mn valence is more complicated, while $M(H, T)$ at $T < 10$ K is far from free-ion behavior, revealing the importance of collective phenomena along the quasi-one-dimensional Li/Mn polyhedral chains at the lowest temperatures.

II. METHODS

We grew single crystals of $Li_2Mn_2(MoO_4)_3$ as large as $5 \times 1 \times 1$ mm^3 from a molten eutectic solution of commercial MnO, Li_2MoO_4, and MoO_3 powders along the experimentally determined Li_2O-MoO_3 pseudobinary line [16]. *In situ* x-ray scattering experiments informing the crystal growth process were performed at the National Synchrotron Light Source II XPD beamline (28-ID-2) with an incident wavelength $\lambda = 0.18202$ Å. The *in situ* measurements were carried out on premixed powders sealed in air in 3-mm-o.d., 2-mm-i.d. quartz capillaries, with the sample position constrained by quartz rods. Samples were heated with a hot-air blower from 300 to 973 K at 0.2 K/s until melting was observed and subsequently cooled from 973 to 773 K at 0.033 K/s to probe the crystal growth process. Once ideal growth temperatures had been identified, further *ex situ* crystal synthesis routines were undertaken in 3N Ag tubing to avoid quartz devitrification observed when samples were exposed to elevated temperatures for dozens of hours. As a precaution, x-ray fluorescence

measurements carried out with a Niton FXL x-ray florescence spectrometer were unable to detect any Ag impurity in the resulting crystals with an estimated detection floor on the order of 10 ppm. The crystals were transparent yellow and rodlike in habit and could be mechanically extracted from the oxide regulus.

We determined the crystal structure of $Li_2Mn_2(MoO_4)_3$ with an Oxford Gemini single-crystal diffractometer with Mo $K\alpha$ radiation. Some 59 815 reflections were collected with 99.4% completeness at $T = 297$ K, of which 2968 independent reflections were used to solve the structure via a charge-flipping algorithm [17–19]. We collected UV/Vis diffuse reflectance spectra with photon energies $h\nu = 1.38$ to 4.96 eV in a Cintra 40 double-beam spectrometer equipped with an integrating sphere coated with $BaSO_4$. The resolution in λ was 1.0 nm. We performed measurements of DC magnetization M on a 2.64-mg collection of single crystals enclosed within a gold sachet via a Quantum Design magnetic property measurement system from temperature $T = 1.8$ to 300 K. Magnetic measurements were carried out in both zero-field-cooled (ZFC) and field-cooled (FC) conditions.

III. RESULTS AND DISCUSSION

A. *In situ* crystal growth optimization

Optimizing *de novo* growth processes to obtain large, high-quality single crystals from solution is a labor-intensive process that may require months of work in the laboratory. For the present system, we identified an ideal composition, $(MnO)_{10}(Li_2MoO_4)_{49.5}(MoO_3)_{51.5}$, from oxide phase diagram literature [16,20] and carried out preliminary *ex situ* experiments to verify crystal formation, which resulted in submillimeter crystals readily identified by their yellow color. Then, as shown in Fig. 1, we carried out an 8-h series of *in situ* x-ray scattering measurements in which we observed the melting of the oxide solution and the resultant precipitation and growth of the desired crystalline phase, permitting us to tune the growth temperature range via a single experiment.

Figure 1(a) shows the scattered intensities of this series of *in situ* measurements. At $T = 373$ K (the onset of the experiment), we observe diffracted peaks corresponding to three phases: rhombohedral $R\bar{3}h$-type Li_2MoO_4, which is best identified by peaks at $Q = 1.37$, 1.52, and 1.76 Å^{-1}; $Pnma$-type MoO_3, best characterized by peaks at $Q = 1.63$ and 1.95 Å^{-1}; and $Fm\bar{3}m$-type MnO, with peaks seen at $Q = 2.50$, 2.93, and 4.03 Å^{-1}. We see the emergence of new intensity, particularly at $Q = 0.78$ and 1.01 Å^{-1} in the 823 K data set, which we ascribe to the formation of monoclinic $P12_11$-type $Li_2Mo_4O_{13}$. The peaks corresponding to all three initial phases, as well as those of $Li_2Mo_4O_{13}$, simultaneously disappear between $T = 823$ and 873 K, signifying melting of the oxide solution. Coincident with this phase transition, we see the emergence of weak, coherent scattering at $Q = 2.37$, 3.38, and 4.12 Å^{-1}, which is consistent with strong {133}, {226}, and {333} reflections expected from our structure solution of $Li_2Mn_2(MoO_4)_3$ that we discuss below. These $Li_2Mn_2(MoO_4)_3$-derived peaks persist as the flux is heated even to 973 K and then cooled to 773 K as the crystals continue to grow as solubility decreases in concert with
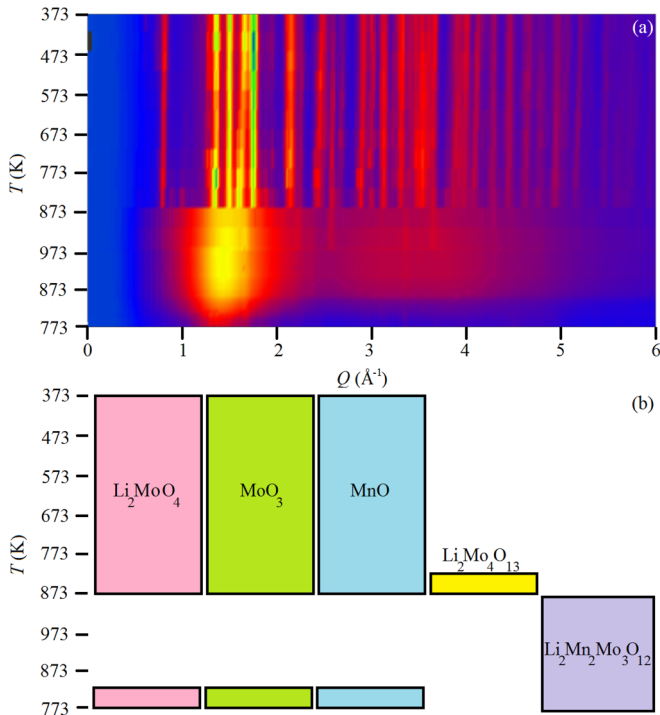
FIG. 1. (a) A color plot of the observed intensities from *in situ* x-ray scattering as a function of the magnitude of the scattering wave vector Q. Experiments were carried out as T was increased from 373 to 973 K with measurements in 50 K increments followed by cooling to 773 K with measurements in 10 K increments, as plotted from top to bottom. Indigo represents low intensity, and the color is incremented in rainbow order from red to orange, yellow, green, and blue as intensity increases. (b) A schematic of the phases present in (a) as a function of temperature as determined by indexing the diffracted peaks.

temperature. Finally, we begin to observe the reemergence of weak oxide peaks, indicating recrystallization of the molten oxide solution at 803 K and below, suggesting that the ideal crystal growth range is 873 → 803 K and allowing us to grow large single crystals for subsequent measurements.

B. Disordered polyhedral chains and charge fluctuations

Figure 2 shows the crystal structure of $Li_2Mn_2(MoO_4)_3$, which consists of three unique, quasi-one-dimensional chains of mixed occupancy Li/Mn positions that are oriented along the crystallographic a direction and mutually connected by vertex-sharing MoO_4 tetrahedra. Our charge-flipping algorithm rapidly and reliably converges to the unit cell shown in Fig. 2(a) with orthorhombic lattice parameters $a = 5.18710(1)$ Å, $b = 10.5856(3)$ Å, $c = 17.8521(4)$ Å, $V = 980.23(4)$ Å^3, and space group *Pnma*, in excellent agreement with previous reports of polycrystalline $Li_{2-2x}Mn_{2+x}(MoO_4)_3$-type compounds and single-crystal $Li_{1.60}Mn_{2.20}(MoO_4)_3$ [21]. Both the quasi-one-dimensional nature of the structure and the mixed occupancy of the Li/Mn sites are more clearly evident in Fig. 2(b), which shows a central $Li_{0.669(3)}Mn_{0.331(3)}O_6$ octahedral chains surrounded by a ringlike structure consisting of $Li_{0.393(2)}Mn_{0.607(2)}O_6$ octahedral chains and chains of $Li_{0.548(4)}Mn_{0.452(4)}O_6$ triangular

prisms. The central chains consist of face-sharing octahedra, as shown in Fig. 2(c), while the ring member chains [Fig. 2(d)] and prisms [Fig. 2(e)] are edge sharing. Refinement yields the overall composition $Li_{2.004(6)}Mn_{1.996(6)}(MoO_4)_3$, which is indistinguishable from an integer occupancy to 0.3% precision. In the solution growth environment, the integer-stoichiometry $Li_2Mn_2(MoO_4)_3$ composition appears to be favored. Our largest crystals were obtained from solutions with excess Li in a 10:1 Li:Mn ratio, and even when we adjusted this ratio, the composition of the resulting crystals remained unchanged. We conclude that during growth the crystals extract the necessary Li from the solution to maintain the favored Mn^{2+} oxidation state.

We considered the possibility that crystallographic disorder associated with mixed Li/Mn occupancy within the three chain structures shown in Fig. 2 could be relieved by lowering the space group symmetry. We would expect such lowering to be easily resolvable given the substantial difference in x-ray scattering cross sections of Li and Mn. Manifestations of lowered symmetry might be a supercell or an incommensurate structural modulation, most likely along the chain direction, i.e., the crystallographic a axis. The $h0\ell$ reciprocal space map shown in Fig. 2(f), however, shows no additional reflections that would be associated with a doubling or tripling of the cell along this direction, nor do we observe such reflections that would accompany an incommensurate structural modulation.

Along these lines, in Figs. 2(g) and 2(h), we show cuts of Fig. 2(f) to clarify the absence of a larger cell or modulated structure. Even with the intensity of the scattered x-rays plotted on a logarithmic scale, we see no evidence of weak peaks that cannot be indexed by the lattice parameters of $Li_2Mn_2(MoO_4)_3$. We do note that the observed odd reflections at (100), (300), (003), (005), and (007) should be systematically absent from the space group *Pnma*. In this case, however, the observed intensity of these peaks is consistent with $\lambda/2$ diffraction of the orders more intense (200), (600), (006), (0010), and (0014) reflections, respectively [22], and we accordingly modeled the effects of $\lambda/2$ contamination in our structural refinement. In any case, a simple doubling of the unit cell in all directions could not alone bring to order the non-half Li/Mn occupancies of the three chains. We likewise considered the possibility of reduced symmetry within a single unit cell by permitting refinement in any of the seven maximally nonisomorphic subgroups of *Pnma*, but in no case did introducing the associated extra degrees of freedom appreciably improve the quality of the refinement. From these results, we conclude that the occupancy of all three Li/Mn polyhedral chains remains statistical, and the structure contains finite chains of the magnetic species in the form of Mn, Mn-Mn, Mn-Mn-Mn, etc., with decreasing likelihood.

It was previously reported that polycrystalline samples could be sintered with various Li/Mn compositions and that submillimeter single crystals with the composition $Li_{1.60}Mn_{2.20}(MoO_4)_3$ could be grown from such presintered polycrystalline precursors [21]. We note that the solution growth procedure we describe here has been successful only in producing crystals with a global Li:Mn ratio indistinguishable from 2:2, despite an approximately 10:1 molar ratio of Li:Mn in the molten growth solution. Elementary
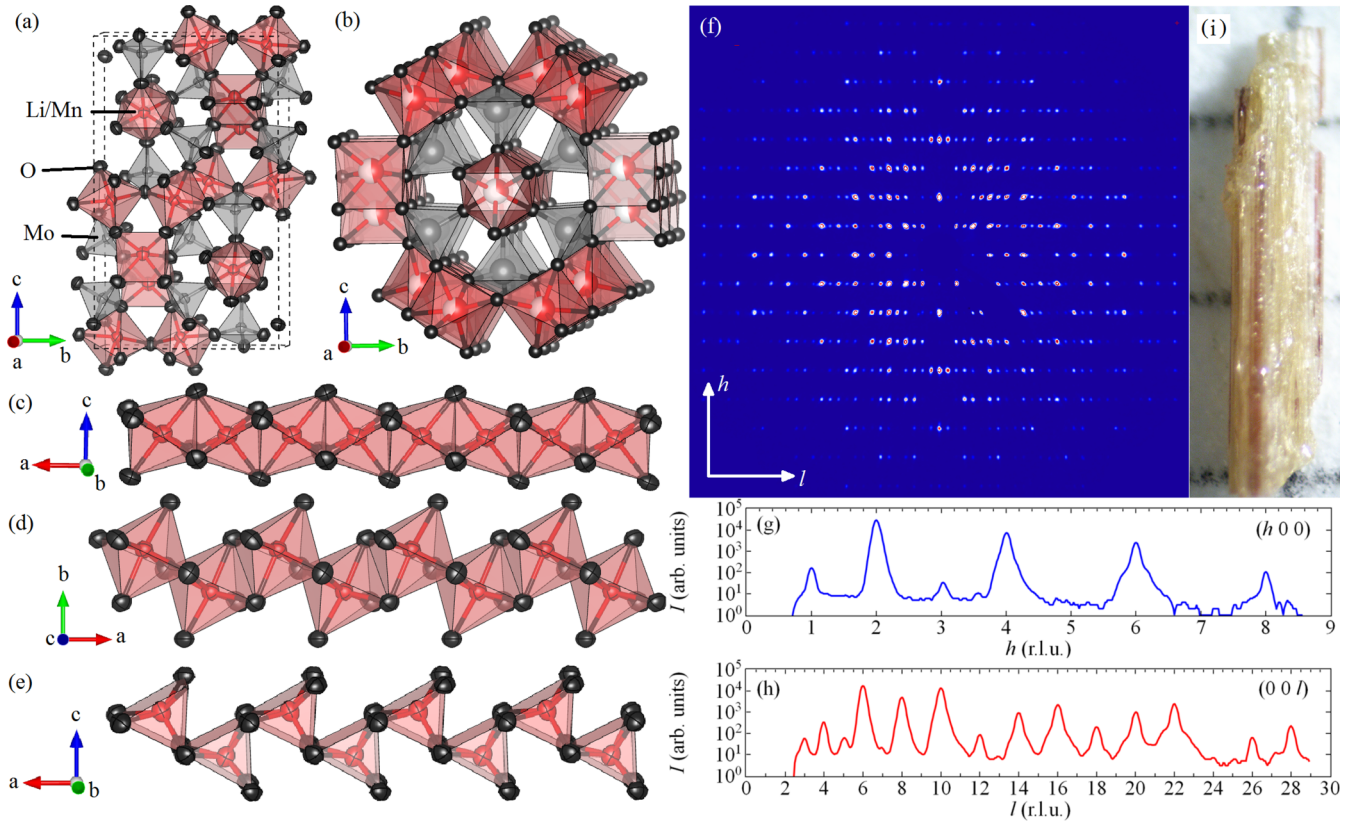
FIG. 2. (a) The unit cell of $Li_{2.004(6)}Mn_{1.996(6)}(MoO_4)_3$ with Li/Mn-centered octahedra and right triangular prisms colored in red, Mo-centered tetrahedra colored in gray, and O drawn in black, as indicated. Refinement was carried out on structure factor F^2, and refinement parameters are residual $R = 0.0336$, weighted residual $wR = 0.0822$, and goodness of fit $S = 2.100$. (b) The primary tubular motif of the structure, consisting of three separated chainlike structures [colors are as in (a)]. (c) The chain consisting of $Li_{0.669(3)}Mn_{0.331(3)}$ face-sharing octahedra [colors are as in (a)]. (d) The chain consisting of the $Li_{0.393(2)}Mn_{0.607(2)}$ edge-sharing octahedra [colors are as in (a)]. (e) The chain consisting of the $Li_{0.548(4)}Mn_{0.452(4)}O_6$ right triangular prisms [colors are as in (a)]. (f) An unwarped image of the $h0\ell$ reciprocal space map with all reflections indexed by lattice parameters showing the absence of a supercell or modulated structure to accommodate disorder. (g) A cut of (f) along $(h00)$ plotted on a logarithmic scale to clarify the absence of a supercell or modulated structure along the direction of the chains. (h) A cut of (f) along the (00ℓ) direction similarly clarifying the absence of a supercell or modulated structure outside the direction of the chains. (i) A typical single crystal on 1-mm grid paper.

valence counting suggests the 2:2 composition is associated with Mn^{2+} and may therefore be the composition made energetically favorable by Hund's stabilization of the Mn $3d^5$ configuration.

Bond valence sums (BVSs) are in agreement to first order with the $3d^5$ picture, but we nevertheless observe substantial discrepancies from the expected integer values. Specifically, BVSs are 2.427(6) for Mn in the $Li_{0.669(3)}Mn_{0.331(3)}$ face-sharing octahedral chains, 2.246(4) for Mn in the $Li_{0.393(2)}Mn_{0.607(2)}$ edge-sharing octahedral chains, and 2.008(4) for Mn in the $Li_{0.548(4)}Mn_{0.452(4)}O_6$ prisms. Thus, even if all Mn BVSs are in reasonably good agreement with the expectation of Mn^{2+}, both octahedra are substantially overbonded. A potential explanation for the discrepancy is that the observed substantial Li occupancies of these two positions lead to shorter bond distances on the local level. Tables of ionic radii typically give Li^{1+} as 90 pm and high-spin Mn^{2+} as 97 pm if both species are octahedrally coordinated, so overbonding at the 5%–10% level is to be expected. The $Li_{0.669(3)}Mn_{0.331(3)}$ face-sharing octahedra, however, are more than 20% overbonded, to an extent that

size effects alone are unable to explain. We conclude that Mn in this system is not precisely divalent and, accordingly, that electroneutrality must require an equivalent valence change elsewhere. In a similar situation, *in situ* x-ray scattering experiments of structurally related $LiCr(MoO_4)_2$ revealed Li intercalation and deintercalation to be accompanied by $Cr^{3+/2+}$ and $Mo^{6+/5+}$ redox, so that overall charges remain balanced [5]. As therefore might be expected, our calculated BVSs for the two tetrahedrally coordinated Mo sites in $Li_2Mn_2(MoO_4)_3$ are 5.815(14) and 5.763(16), despite full Mo occupancy on both sites. This modest underbonding of Mo^{6+} in concert with the substantial overbonding of Mn^{2+} suggests that the valence picture of $(Li^{1+})_{2.004(6)}(Mn^{2+})_{1.996(6)}(Mo^{6+})_3(O^{2-})_{12}$ is not as simple as previously thought and that transition metal valence fluctuations may play a role in the stabilization of the lyonsite crystal structure in this case.

C. Mn^{2+}-like excitations and the charge gap

As we show in Fig. 3, $Li_2Mn_2(MoO_4)_3$ is an insulator with a wide, direct charge gap, and its UV/Vis spectrum is broadly
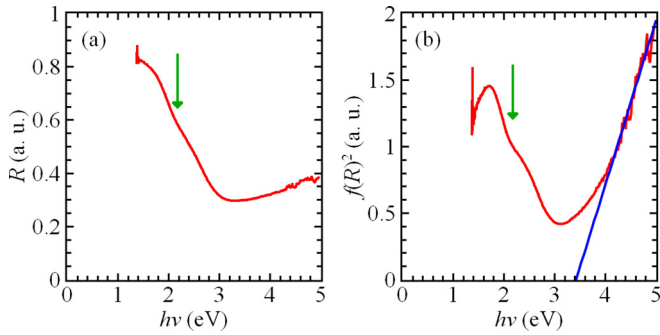
FIG. 3. (a) The UV/Vis diffuse reflectance R spectrum of $Li_2Mn_2(MoO_4)_3$ (red) plotted as a function of incident photon energy $h\nu$ from 1.38 to 4.96 eV, corresponding to wavelength $\lambda = 900$ to 250 nm. The green arrow denotes the position of a likely transition of octahedral Mn^{2+} to its first excited state. (b) The square of the Kubelka-Munk function $f(R)^2$ plotted versus $h\nu$ (red), where the solid blue line is a best fit of the Tauc relation to the linear region (see text).

consistent with the expected localized excitons of a primarily Mn^{2+} state. Figure 3(a) presents the diffuse reflectance R spectrum after background subtraction from a collection of infinitely ($\sim$1 mm) thick crystals with light directed normal to the (001) crystallographic surface. R approaches 1 at incident light energies $h\nu$ below 2 eV, indicating that the crystals are largely transparent to red and near-infrared photons, and falls off broadly as $h\nu$ is increased, most likely as charge carriers are excited across the gap. An inflection in R at 2.0(1) eV is consistent with the transition in binary MnO of octahedrally coordinated Mn^{2+} from the ground state to the first excited quartet state, $^6A_{1g} \rightarrow\, ^4T_{1g}$ [23,24], suggesting that the octahedrally coordinated Mn in $Li_2Mn_2(MoO_4)_3$ are likewise predominantly divalent. This transition is spin forbidden by Pauli exclusion and is therefore accomplished by spin-spin or spin-orbit coupling. The resulting broad shoulder in R around 2.2(2) eV is likely the source of the observed yellow color of the crystals and may be associated with the charge transfer states we infer from BVSs.

Like the presumably $^6A_{1g} \rightarrow\, ^4T_{1g}$ derived inflection at $h\nu = 2.0(1)$, the observed minimum in R near $h\nu = 3$ eV is again consistent with known $d-d$ optical transitions in binary MnO, reinforcing the Mn^{2+} octahedral picture for $Li_2Mn_2(MoO_4)_3$. By comparison to MnO, we infer that the minimum in R corresponds to transitions from the $^6A_{1g}$ ground state to the $^4A_{1g}$ and ^6E_g excited states, which remain degenerate in the octahedral crystal field [25] and are expected at $h\nu = 2.95$ eV [23]. Above 3 eV, R increases again over a wide energy scale of 2 eV and may just reach a maximum near the upper $h\nu$ limit of our measurement, a feature likely associated with the $3d^5 \rightarrow 3d^4 + 4s^1$ transition observed in direct reflectance measurements of MnO [26]. These spectroscopic results are consistent with the excitations expected of localized, octahedrally coordinated Mn^{2+}, although we stress that they do not require a uniform divalent configuration. Even prototypically divalent MnO has substantial d^6 and even d^7 ligand hole character [23,27], and both experimental and theoretical investigations of more complicated materials
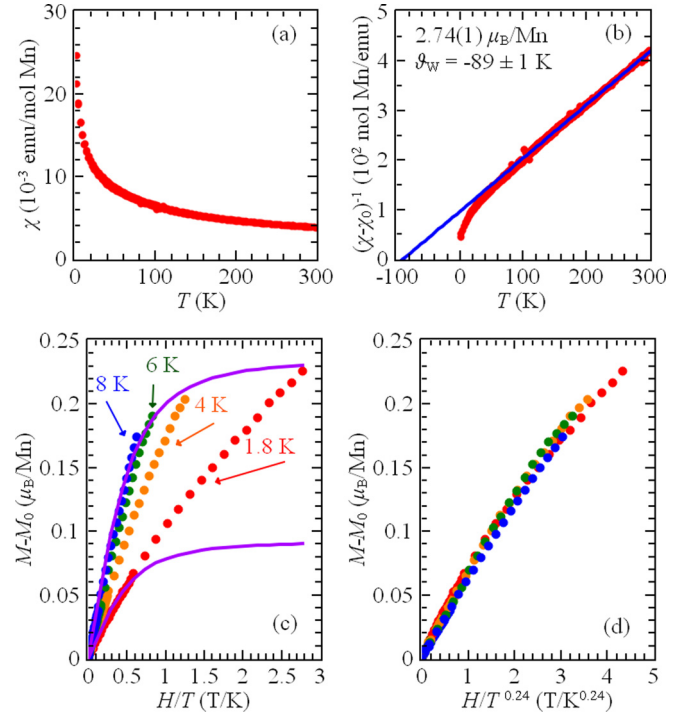

FIG. 4. (a) The temperature T dependence of the dc magnetic susceptibility $\chi = M/H$ with applied field $H = 1000$ Oe of a collection of $Li_2Mn_2(MoO_4)_3$ single crystals (red circles). Measurements carried out in FC and ZFC configurations are overlaid and indistinguishable. (b) The T dependence of $1/(\chi - \chi_0)$ (red circles), where χ_0 is the sum of T-independent contributions to χ. The blue solid line is a fit to the Curie-Weiss law for $T > 100$ K, corresponding to a fluctuating moment of $2.74(1)\mu_B/Mn$ and Weiss temperature $\theta_W = -89 \pm 1$ K, as indicated. (c) Magnetization $M - M_0$ plotted as a function of H/T to illustrate deviation from Brillouin-function-like behavior. M_0 is the temperature-independent contribution to M as in (b). Colors are $T = 1.8$ K (red), 4 K (orange), 6 K (green), and 8 K (blue), as indicated. The upper and lower solid violet lines are the $g = 2$, $J = 5/2$ Brillouin function with magnitude arbitrarily adjusted to the $T = 8$ K and $T = 1.8$ K data, respectively. (d) $M - M_0$ plotted as a function of H/T^γ with the critical exponent $\gamma = 0.24(3)$ [colors are as in (c)].

reveal even greater charge fluctuations in otherwise ostensibly Mn^{2+} systems [28–31].

The square of the Kubelka-Munk function $f(R)^2$ plotted in Fig. 3(b) permits us to estimate the magnitude of optical charge gap of $Li_2Mn_2(MoO_4)_3$ as $E_g = 3.43(12)$ eV. We found lines of best fit tangent to $f(R)^2$ for $h\nu > 4.05$ eV via linear regression to the Tauc relation $\alpha h\nu = C(h\nu - E_g)^\beta$ for absorption coefficient α and a sample geometry-dependent fitting parameter C. The nature of the allowed transitions across the gap determines the value of the exponent β in this expression, with $\beta = 1/2$ corresponding to direct transitions and $\beta = 2$ corresponding to indirect ones. For $Li_2Mn_2(MoO_4)_3$, the regression is substantially improved when $\beta = 1/2$, suggesting that the optical gap is direct.

D. Disorder and correlated magnetic fluctuations

Magnetic measurements presented in Fig. 4 further dispel the simple picture of independent local moments in

fixed-valent $(Li^{1+})_2(Mn^{2+})_2(Mo^{6+})_3(O^{2-})_{12}$. As expected of a Curie-Weiss paramagnet, the dc magnetic susceptibility $\chi = M/H$ shown in Fig. 4(a) falls off rapidly as T is increased from our 1.8 K base temperature. A non-negligible temperature-independent contribution $\chi_0 = 1.4 \times 10^{-3}$ emu/mol Mn remains present across the entire measurement, presumably the sum of Van Vleck and core diamagnetic terms. Once χ_0 is subtracted, the remaining susceptibility corresponds to the Curie Weiss law $\chi - \chi_0 = C/(T + \theta_W)$, as shown in Fig. 4(b), where the magnitude of the effective fluctuating moment is derived from the Curie constant C and θ_W is the Weiss temperature. The fit of this relation is in excellent agreement with the data for $T > 100$ K, yielding a fluctuating moment of only $2.74(1)\mu_B$/Mn, less than half the $5.9\mu_B$ expected for the Mn^{2+} free ion. This moment is notably less than even the $4.9\mu_B$ expected for the Mn^{3+} free ion. Observation of both static and fluctuating moments substantially less than free-ion values is not atypical in superficially Mn^{2+}-based insulators, for example, LaMnPO [28], CaMn$_2$Sb$_2$ [32,33], LaMnAsO [34], and BaMn$_2$As$_2$ [35,36]. Factors responsible for reduction of magnetic moments in these systems include valence fluctuations [28,29], effective dimensionality [37], and orbital hybridization, the first two of which our crystallographic and spectroscopic measurements suggest to be important in Li$_2$Mn$_2$(MoO$_4$)$_3$.

In addition to these departures on the local scale from Mn^{2+} physics, $\chi(T)$ suggests that the substitutional disorder observed in our crystallographic characterization plays a role in frustrating the onset of the eventual magnetic phase. Specifically, $\theta_W = -89 \pm 1$ K is nearly two orders of magnitude above the reported ordering temperature 1.4 K [14], indicating a significant suppression of magnetic order that may originate from the inherent chemical disorder of the three Li/Mn polyhedrally coordinated sites. The prevailing magnetic fluctuations are antiferromagnetic in nature, as indicated by $\theta_W < 0$, in agreement with the previous report. The magnitude of θ_W that we determined from $\chi(T)$ is somewhat higher than was previously obtained from ESR measurements carried out on polycrystalline powders ($\theta_W = -56$ to -65 K) [14]. This observation is in line with our expectation of higher θ_W in single-crystal samples, which by definition lack the grain boundaries and associated impurities that typically reduce θ_W [38]. We conclude that the absence of magnetic order between our base temperature $T = 1.8$ K and $-\theta_W = 89 \pm 1$ K is unrelated to grain boundaries, contamination, or issues of crystal quality and instead stems from intrinsic crystallographic disorder that persists to the unit cell level. In the complete absence of such chemical disorder and frustration, one would expect Li$_2$Mn$_2$(MoO$_4$)$_3$ to transition to a long-range antiferromagnetic phase with T_N on the order of 100 K.

On the other hand, measurements of M below $T = 10$ K demonstrate that the dominant magnetic excitations at the lowest temperatures are definitively not those of local paramagnetic moments, regardless of Mn atomic configuration. We plot in Fig. 4(c) M after subtracting the same T-independent term $M_0 = \chi_0 H$ as in Fig. 4(b). The remaining quantity $M(H, T) - M_0$ is invariably far from saturation, reaching only $0.23\mu_B$/Mn even at $T = 1.8$ K and $H = 5$ T. The Brillouin

function, which describes the magnetization of local paramagnetic moments as a function of H and T, would be 99% saturated at these values of $T = 1.8$ K and $H = 5$ T, clearly in stark disagreement with our observations. Additionally, as Fig. 4 shows, the scaling of $M - M_0$ with the quantity H/T expected for independently fluctuating local moments is nearly completely absent. We must conclude that the Mn moments in Li$_2$Mn$_2$(MoO$_4$)$_3$ are correlated and that the observed fluctuations are instead the result of collective phenomena, presumably stemming from the onset of the magnetic transition reported previously at 1.4 K [14]. We note that our measurements of $\chi(T \geqslant 1.8$ K$)$ show no evidence of reaching this transition, which could occur at a temperature higher than 1.4 K in single-crystal samples. Furthermore, the absence of a Brillouin-like contribution to M indicates that none of the three crystallographically independent, quasilinear sublattices of Mn [Figs. 2(c)–2(e)] host individually fluctuating moments, suggesting that all three may participate in this eventual transition.

Our subsequent scaling analysis shown in Fig. 4(d) suggests a strong one-dimensional character to these correlated fluctuations above the eventual ordering temperature. As Fig. 4(d) demonstrates, $M - M_0$ scales as H/T^γ with $\gamma = 0.24(3)$ instead of the H/T dependence expected of independently fluctuating local moments. We note that there is no qualitative change in this result if we take $M_0 = 0$ as a sanity check. We recently observed similar phenomena, albeit with a larger value of $\gamma = 0.68(4)$, in Bi$_2$CrAl$_3$O$_9$ [39]. In that case, the sole magnetic ion Cr^{3+} is octahedrally coordinated by O, and disordered, quasi-one-dimensional chains of magnetic Cr- and nonmagnetic Al-centered, edge-sharing octahedra are arrayed along a single crystallographic direction, much like the chains of Li- and Mn-centered polyhedra we find in Li$_2$Mn$_2$(MoO$_4$)$_3$. The apparent absence of any Cr/Al occupancy ordering along the octahedra of the former system leads to finite chains of Cr-centered octahedra with statistically varying lengths, which form the fundamental magnetic unit and manifest in $M(H, T)$ as $\gamma < 1$.

As a point of comparison, $\gamma < 1$ is found throughout the disordered phase of so-called random transverse-field Ising spin chains (RTISCs). RTISCs are exactly soluble in both ordered and disordered phases across a wide range of parameters [40,41], which makes for a convenient theoretical approximation to experimentally accessible systems like Bi$_2$CrAl$_3$O$_9$ and Li$_2$Mn$_2$(MoO$_4$)$_3$. Specifically, χ diverges in disordered RTISCs at low temperatures as $\chi(T) \sim 1/T^\gamma$ ($\gamma < 1$), suggesting that M adopts a universal function of H/T^γ, just as we observe in Li$_2$Mn$_2$(MoO$_4$)$_3$ in Fig. 4(d). These results to not imply Li$_2$Mn$_2$(MoO$_4$)$_3$ is an RTISC by any means but merely that compositional disorder and low dimensionality, as we find from our crystallographic measurements, are potential roots of the H/T^γ dependence. In true RTISC systems, γ varies continuously with a parameter δ that quantifies the system's distance from criticality with $\gamma = 0$ at the QCP. If the same arguments can be applied to Bi$_2$CrAl$_3$O$_9$ and Li$_2$Mn$_2$(MoO$_4$)$_3$, the smaller $\gamma = 0.24(3)$ we find for the latter would imply that this system is more weakly disordered, which is perhaps consistent with the Li/Mn occupancies of the individual chains being further from Cr$_{0.50}$Al$_{0.50}$, as

observed in the former. Regardless of whether such a comparison can be made, it appears that $M(H/T^\gamma)$ in $Li_2Mn_2(MoO_4)_3$ arises from a superposition of the thermal and quantum fluctuations of an ordered state, frustrated by chemical disorder, that coalesces only below $T < 1.8$ K.

IV. CONCLUSIONS

The growth of large crystals of $Li_2Mn_2(MoO_4)_3$ was facilitated and accelerated by *in situ* x-ray scattering measurements that identified the onset of nucleation, clarified the ideal growth temperature range, and demonstrated a path to avoid the nucleation of unwanted secondary phases, which could potentially derail magnetic characterization. The crystals resulting from the optimized synthesis routine were large enough for spectroscopic characterization and for magnetic measurements even in a paramagnetic system with a small moment far from saturation at large fields.

Accordingly, we report that $Li_2Mn_2(MoO_4)_3$ is an insulator with a 3.43(12)-eV direct charge gap. Elementary charge counting suggests an Mn^{2+} valence state, which is supported by previous ESR measurements. Moreover, this state is consistent with the excitations we observed in UV/Vis spectroscopy, paralleling those of the prototypical divalent system MnO. The full picture is more complicated, however, as is the case for other ostensibly divalent Mn-based insulators, including MnO itself. *Ex situ* single-crystal x-ray diffraction measurements revealed substantial overbonding of two of the Mn positions, accompanied by underbonding of Mo, suggesting that the system hosts considerable charge fluctuations. These fluctuations are borne out in magnetic measurements that reveal a high-temperature fluctuating moment less than half the value expected of the Mn^{2+} free ion. Across the various lyonsite-structured and related materials, nature compromises when necessary to preserve the structure type by introducing substitutional disorder between the alkali metal and transition metal sites. When this compromise is circumvented with large-radii alkali metals, the structure is forced to distort. We posit that charge fluctuations may be

another, perhaps concurrent, avenue towards stabilizing the apparently fragile lyonsite structure.

The magnetic properties of $Li_2Mn_2(MoO_4)_3$ likewise revealed the importance of chemical disorder in frustrating the magnetic ordering temperature far below θ_W. Instead of ideal, long-range antiferromagnetism, we detected finite, correlated chains of magnetic ions collectively fluctuating above an eventual ordered state that occurs only below $T < 1.8$ K. $Li_2Mn_2(MoO_4)_3$ appears to be a member of a broader class of finite magnetic chain systems potentially identifiable by H/T^γ scaling with $\gamma < 1$ at sufficiently low T, which may extend across a wide variety of compositions and structure types. It remains to be seen if a QCP associated with $\gamma \to 0$ and controlled by disorder can be realized experimentally in this class of materials.

[1] L. Balents, Nature (London) **464**, 199 (2010).

[2] L. S. Wu, W. J. Gannon, I. A. Zaliznyak, A. M. Tsvelik, M. Brockmann, J.-S. Caux, M. S. Kim, Y. Qiu, J. R. D. Copley, G. Ehlers, A. Podlesnyak, and M. C. Aronson, Science **352**, 1206 (2016).

[3] K. Feng, F. Wang, H. Zhang, X. Li, and H. Zhang, J. Mater. Chem. A **6**, 19107 (2018).

[4] M. Sonni, M. F. Zid, and C. Issaoui, J. Solid State Chem. **272**, 244 (2019).

[5] K. Feng, F. Wang, X. Yang, H. Zhang, X. Li, and H. Zhang, J. Mater. Chem. A **7**, 567 (2019).

[6] K. M. Hercule, Q. Wei, O. K. Asare, L. Qu, A. M. Khan, M. Yan, C. Du, W. Chen, and L. Mai, Adv. Energy Mater. **5**, 1500060 (2015).

[7] J. P. Smit, P. C. Stair, and K. R. Poeppelmeier, Chem. Eur. J. **12**, 5944 (2006).

[8] D. E. Bugaris and H.-C. zur Loye, Acta Crystallogr. C **68**, i34 (2012).

[9] A. Sarapulova, D. Mikhailova, A. Senyshyn, and H. Ehrenberg, J. Solid State Chem. **182**, 3262 (2009).

[10] M. Alvarez-Vega, U. Amador, and M. E. Arroyo-de Dompablo, J. Electrochem. Soc. **152**, A1306 (2005).

[11] W. M. Reiff, J. H. Zhang, and C. C. Torardi, J. Solid State Chem. **62**, 231 (1986).

[12] S. Hayashida, D. Blosser, K. Yu. Povarov, Z. Yan, S. Gvasaliya, A. N. Ponomaryov, S. A. Zvyagin, and A. Zheludev, Phys. Rev. B **100**, 134427 (2019).

[13] M. Hase, A. Matsuo, K. Kindo, and M. Matsumoto, Phys. Rev. B **96**, 214424 (2017).

[14] N. M. Suleimanov, S. R. S. Prabaharan, S. M. Khantimerov, F. A. Nizamov, M. S. Michael, H. Drulis, and P. Wisniewski, Appl. Phys. A **122**, 754 (2016).

[15] I. Jendoubi, M. Ptak, A. Pikul, J. Chmielowiec, A. Ciupa, M. Maczka, and M. F. Zid, J. Solid State Chem. **277**, 738 (2019).

[16] M. Moser, D. Klimm, S. Ganschow, A. Kwasniewski, and K. Jacobs, Cryst. Res. Technol. **43**, 350 (2008).

[17] V. Petříček, M. Dušek, and L. Palatinus, Z. Kristallogr. **229**, 345 (2014).

[18] L. Palatinus and G. Chapuis, J. Appl. Crystallogr. **40**, 786 (2007).

[19] K. Momma and F. Izumi, J. Appl. Crystallogr. **44**, 1272 (2011).

[20] *Phase Equilibria Diagrams Online Database*, NIST Standard Reference Database Vol. 31 (American Ceramic Society, Westerville, Ohio, 2019).

[21] S. F. Solodovnikov, Z. A. Solodovnikova, R. F. Klevtsova, L. A. Glinskaya, P. V. Klevtsov, and E. S. Zolotova, J. Struct. Chem. **35**, 871 (1994).

[22] C. G. Gianopoulous, Z. Chua, V. V. Zhurov, and A. A. Pinkerton, J. Appl. Crystallogr. **50**, 643 (2017).

[23] J. van Elp, R. H. Potze, H. Eskes, R. Berger, and G. A. Sawatzky, Phys. Rev. B **44**, 1530 (1991), and references therein.

[24] S. Sugano, Y. Tanabe, and H. Kamimura, *Multiplets of Transition-Metal Ions in Crystals* (Academic, New York, 1970).

[25] G. W. Pratt and R. Coelho, Phys. Rev. **116**, 281 (1959).

[26] L. Messick, W. C. Walker, and R. Glosser, Phys. Rev. B **6**, 3941 (1972).

[27] J. A. Schiller, L. K. Wagner, and E. Ertekin, Phys. Rev. B **92**, 235209 (2015).

[28] J. W. Simonson, Z. P. Yin, M. Pezzoli, J. Guo, J. Liu, K. Post, A. Efimenko, N. Hollmann, Z. Hu, H. J. Lin, C. T. Chen, C. Marques, V. Leyva, G. Smith, J. W. Lynn, L. Sun, G. Kotliar, D. N. Basov, L. H. Tjeng, and M. C. Aronson, Proc. Natl. Acad. Sci. U.S.A. **109**, E1815 (2012).

[29] J. A. Kurzman, A. J. Martinolich, and J. R. Neilson, Phys. Rev. B **92**, 184414 (2015).

[30] E. Beyreuther, S. Grafström, L. M. Eng, C. Thiele, and K. Dörr, Phys. Rev. B **73**, 155425 (2006).

[31] A. Walsh, A. A. Sokol, J. Buckeridge, D. O. Scanlon, and C. R. A. Catlow, Nat. Mater. **17**, 958 (2018).

[32] J. W. Simonson, G. J. Smith, K. Post, M. Pezzoli, J. J. Kistner-Morris, D. E. McNally, J. E. Hassinger, C. S. Nelson, G. Kotliar, D. N. Basov, and M. C. Aronson, Phys. Rev. B **86**, 184430 (2012).

[33] D. E. McNally, J. W. Simonson, J. J. Kistner-Morris, G. J. Smith, J. E. Hassinger, L. DeBeer-Schmitt, A. I. Kolesnikov, I. A. Zaliznyak, and M. C. Aronson, Phys. Rev. B **91**, 180407(R) (2015).

[34] M. A. McGuire and V. O. Garlea, Phys. Rev. B **93**, 054404 (2016).

[35] Y. Singh, M. A. Green, Q. Huang, A. Kreyssig, R. J. McQueeney, D. C. Johnston, and A. I. Goldman, Phys. Rev. B **80**, 100403(R) (2009).

[36] D. E. McNally, S. Zellman, Z. P. Yin, K. W. Post, H. He, K. Hao, G. Kotliar, D. Basov, C. C. Homes, and M. C. Aronson, Phys. Rev. B **92**, 115142 (2015).

[37] M. Zingl, E. Assmann, P. Seth, I. Krivenko, and M. Aichhorn, Phys. Rev. B **94**, 045130 (2016).

[38] A. Yu. Emelyanov, N. A. Pertsev, S. Hoffmann-Eifert, U. Böttger, and R. Waser, J. Electroceram. **9**, 5 (2002).

[39] J. C. Umana, A. M. Baccarella, L. Steinke, A. Geritano, Y. Janssen, M. C. Aronson, and J. W. Simonson, Phys. Rev. B **100**, 104425 (2019).

[40] D. S. Fisher, Phys. Rev. B **51**, 6411 (1995).

[41] F. Iglói and C. Monthus, Phys. Rep. **412**, 277 (2005).